Research Square

Preprints are preliminary reports that have not undergone peer review.
They should not be considered conclusive, used to inform clinical practice,
or referenced by the media as validated information.

A new screen-printed carbon sensor decorated gold nanoparticles/kaolinite mineral: electrochemical analysis of Propyphenazone and the investigation of ds-DNA interaction

Ceren Yıldız
Ankara University
Dilek Eskiköy Bayraktepe
Ankara University
Zehra Yazan (zdurmus@science.ankara.edu.tr)
Ankara University

Research Article

Keywords: Propyphenazone, Kaolinite mineral, Gold nanoparticles, Screen printed electrode, Voltammetry, DNA interaction

Posted Date: August 21st, 2023

DOI: https://doi.org/10.21203/rs.3.rs-3262598/v1

License: This work is licensed under a Creative Commons Attribution 4.0 International License.
Read Full License

Abstract

This work represents the development of natural kaolinite mineral (Kao)–gold nanoparticles (GNPs) modified screen-printed carbon electrode (SPCE) based on biocompatible electrode material for the electrochemical quantification of Propyphenazone (PROP) and the investigation of the interaction between PROP and ds-DNA. The surface characteristics of the Kao–GNPs/SPCE were examined by Cyclic Voltammetry (CV), Electrochemical Impedance Spectroscopy (EIS), and Field-Emission Scanning Electron Microscopy (FE-SEM) with Energy Dispersive X-ray Spectroscopy (EDS) methods. The effect of Kao and gold compositions, pH, and interferences studied the analytical performance of this sensor. PROP has an irreversible oxidation signal on Kao–GNPs/SPCE sensor surface. Based on this oxidation signal, calibration works were carried out using differential pulse voltammetry (DPV), and linear working range, LOD, and LOQ were determined. The real sample analysis of PROP was implemented in human serum samples with a recovery value of 99.43%. Binding constant (K) and Gibbs free energy change (ΔG°) relating to the interaction between PROP and ds-DNA were calculated to be 2.14 (± 0.42) × 10^4 M^{-1} and −24.70 kJ mol^{-1}, respectively.

1 Introduction

Propyphenazone (PROP), 1,2-dihydro-1,5-dimethyl-4-(1-methyl ethyl)-2-phenyl-3H-pyrazol-3-one, has analgesic, anti-inflammatory, and antipyretic properties. It was initially patented in 1931 and derived from the phenazone group. PROP is used in a number of analgesic combinations in many countries. It is marketed as a combination formulation with paracetamol and caffeine to treat some pains such as headache, muscular aches, neuralgia, backache, joint pain, rheumatic pain, migraine, general pain, toothache, and menstrual pain [1, 2]. It has adverse effects when consumed to overdose, such as tiredness, nausea, headache, dizziness, etc. [3]. Fetotoxicity was 21.0 mg/kg per day for PROP [2]. Monitoring serum levels of PROP is necessary for human health. To this end, several analytical methods have been developed for analyzing related drugs, including chromatography [4, 5] and spectroscopy [6]. Though there is only one electrochemical simultaneous analysis procedure of PROP with paracetamol and caffeine, there is no detailed individual electrochemical analysis procedure of PROP in the literature reports. For this purpose, the individual electroanalytical determination method and the interaction of PROP with ds-DNA have been suggested with current work by using the differential pulse voltammetric technique (DPV). Compared to conventional analytical methods, voltammetric techniques have some advantages, like being an affordable, simple, fast response, easy to use, selective, and sensitive [7]. The sensitivity and selectivity of a voltammetric method are highly based on the working electrode system. Several types of carbon-based-working electrodes have been used in voltammetric techniques, such as carbon paste, glassy carbon, pencil graphite, boron-doped diamond, and screen-printed electrodes [8, 9]. Among them, screen-printed carbon electrodes (SPCEs) have a single use, portability, fast, selectivity, and sensitivity compared to the others [10]. The modification of SPCEs is suitable for specific catalytic reactions, sensitivity, and selectivity. In this modification, carbon nanotubes, conducting polymers, noble metal nanoparticles, and clay minerals have been used [11–14]. Among them, clay minerals such as

kaolinite, smectite, illite, chlorite, attapulgite, and sepiolite are the hydroxylated and hydrated aluminum, iron and/or magnesium silicates. Clay minerals have similar chemical compositions but different crystal structures [15]. Kaolinite mineral with the chemical formula, $Al_2Si_2O_5(OH)_4$ is a dioctahedral formed by the 1:1 stacking of tetrahedral and octahedral layers [16]. Kaolinite modified on the electrode surface possesses tremendous adsorption capacity, large surface area, increasing analyte sensitivity, and chemical stability [17].

Clay minerals and gold nanoparticles (GNPs) are hybridized to produce remarkable composite materials with strong electrochemical conductivity, an excessive surface-to-volume ratio, high chemical reactivity, and the capability to chemisorb various types of molecules. The combination of clay minerals and gold nanoparticles provides extraordinary composite materials with strong electrochemical conductivity, large surface-to-volume ratio, high chemical reactivity, large working concentration ranges, and the ability to absorb various molecules chemically [18]. The current work offers the first use of GNPs and Kao mineral composite to modify the surface of the SPCE for sensitive voltammetric analysis of PROP.

Investigating DNA-drug interactions plays an important role in new drug design, controlling gene activity, and some cellular processes [19]. For this purpose, the binding mode and the binding constant (K) of the PROP-(ds-DNA) complex formation were also calculated for the first time.

2 Experimental

2.1 Chemicals and solutions

The standard powder of Propyphenazone was supplied from Atabay Drug Company, Istanbul, Turkiye. $HAuCl_4$, H_2SO_4, chitosan, acetic acid, sodium hydroxide, KCl, HCl, $K_4Fe(CN)_6$, $K_3Fe(CN)_6$, and sodium salt of ds-DNA were purchased from Sigma-Aldrich Company. Kaolinite mineral (KH Kaolen) was supplied by ESAN Eczacıbaşı (Istanbul, Turkey). The chemical compositon is as follow: SiO_2: 62.70%; Al_2O_3: 25.34%; Fe_2O_3: 0.621%; TiO_2: 0.81%; CaO: 0.10%; MgO: 0.10%; Na_2O: 0.08%; K_2O: 0.18%.

The 10.0 mM stock solution of PROP was prepared by dissolving a known amount of standard propyphenazone powder in a water-ethanol mixture (1:1). The 1000 ppm stock ds-DNA solution was prepared by dissolving 5.0 mg sodium salt of ds-DNA in 5.0 mL distilled water and based on the literature, the molar concentration of ds-DNA was determined using UV-Visible spectroscopy method [20, 21]. 1.0 M acetate buffer solution (ABS) was prepared by mixing concentrated acetic acid and 1.0 M NaOH. The pH of the buffer (pH 4.0–6.0) was adjusted with 1.0 M NaOH solution. The 1% (w/v) chitosan solution was prepared by dispersing a known amount of chitosan powder in 2% (v/v) acetic acid solution by stirring on a magnetic plate for 1 hour.

2.2 Apparatus

All electrochemical measurements (CV, DPV, and EIS) were recorded by Palmsens*4* potentiostat/galvanostat system (from Holland). The screen-printed carbon electrode (DRP-110),

consisting three-electrode system, was used with a Palmsens electrode connector. All pH measurements were carried out using a HANNA/HI2211 pH/ORPmeter (LABOR, Istanbul, Turkey), and double-distilled water was supplied from the Mpminipure water distillation system (MES Turkey). UV-Visible measurements were done by Shimadzu1700 UV–Vis spectrophotometer (Shimadzu, Tokyo, Japan) with 1×1 cm quartz cells. FE-SEM images were recorded by Quanta FEG 250 Scanning Electron Microscope (Holland) with 20 KeV electron acceleration voltage.

2.3 Preparation of Kao–GNPs/SPCE

The preparation of the Kao–GNPs/SPCE sensor has two steps:

The SPCE surface was deposited with gold nanoparticles via the electrodeposition method in the first step. To this end, successive 15-cycle CV voltammograms of 0.05 mM $HAuCl_4$ with a scan rate of 50 mVs^{-1} in 0.05 M H_2SO_4 (pH 2.0) were recorded in the (– 0.2) – (+ 1.3) V potential range (Supplementary File, Fig. S1). This figure shows an oxidation signal at about 0.8 V and a reduction signal at about 0.3 V. It was attributed to oxidation/reduction signals of gold [22]. Moreover, the increase in the oxidation and reduction current signals confirms the formation of GNPs on the surface [23]. In the second step, the Kao mixture (1.0% w/v) was prepared by dispersing Kao clay in a chitosan solution by stirring on a magnetic plate for 1 hour. Then, 9.0 µL of the mixture was dropped onto the GNPs/SPCE surface to form Kao–GNPs/SPCE sensor and dried at room temperature for about 1 hour.

2.4 Real sample preparation

A serum sample (H4522, from human male AB plasma, USA origin, sterile-filtered) was obtained from Sigma Aldrich. Serum samples were stored at − 20°C and used without any pre-treatment. For the preparation of samples, the frozen serum sample was defrosted at room temperature. The 10.0 µL sample was spiked into the solution containing 30.0 µM PROP in acetate buffer, pH 4.5. The differential pulse voltammograms were recorded. The obtained results were used for calibration and recovery studies.

3 Results and Discussion

3.1 Characterization of Kao–GNPs/SPCE

The surface morphological characterization of the sensors was investigated by FE-SEM and EDS methods. FE-SEM images of bare SPCE, GNPs/SPCE, Kao/SPCE, and Kao–GNPs/SPCE are given in Fig. 1. Bare SPCE has a relatively smooth structure (Fig. 1a) compared to the others. In the case of modifying with gold nanoparticles, the nano-sized gold nanoparticles are visible on the surface of SPCE (Fig. 1b). After modification with Kao, the sensor surfaces gain a rough and 3D structure (Fig. 1c and d). Figure 1e represents the EDS spectra of Kao–GNPs/SPCE, and the existence of Au, Al, Si, Na, C, O, and N signals in the spectrum confirm the formation of gold nanoparticles and coating of Kao clay on the SPCE surface.

The electrochemical characterization of the sensors was investigated with CV and EIS methods using a 5.0 mM $Fe(CN)_6^{3-/4-}$ redox probe in 0.1 M KCl solution. CV voltammograms are given in Fig. 2a. The highest anodic and cathodic peak currents of 5.0 mM $Fe(CN)_6^{3-/4}$ were recorded on Kao–GNPs/SPCE sensor surface (red line) compared to bare SPCE (blue line), GNPs/SPCE (yellow line), and Kao/SPCE (green line). It was attributed to the combination of the large adsorption capacity of Kao and the superior conductivity of gold nanoparticles.

Nyquist diagrams of bare SPCE (blue line), GNPs/SPCE (yellow line), Kao/SPCE (green line), and Kao–GNPs/SPCE (red line) are demonstrated in Fig. 2b. The R_{ct} values of these sensors were estimated by an equivalent circuit (Z Circuit Fitting software in Palmsen*4*) and calculated as 366 Ω, 257 Ω, 32.58 Ω, and 3.64 Ω, respectively. These obtained R_{ct} values indicate the higher electron transfer rate on Kao–GNPs/SPCE. The active surface areas of SPCE, GNPs/SPCE, Kao/SPCE, and Kao–GNPs/SPCE were calculated using the Randles-Sevcik equation [24]. It was found to be 0.159 (± 0.0060) cm^2 for SPCE, 0.183 (± 0.0003) cm^2 for GNPs/SPCE, 0.374 (± 0.0010) cm^2 for Kao/SPCE and 0.444 (± 0.0035) cm^2 for Kao–GNPs/SPCE. Compared to the bare SPCE, Kao–GNPs/SPCE has a nearly 2.8-fold higher surface area.

The electrochemical oxidation response of 30.0 µM PROP was recorded by the DPV method in acetate buffer solution, pH 4.5 on the surface of the modified electrodes (Fig. 3). One anodic oxidation peak appeared at about 0.65 V on the surface of the SPC electrode. After the modification GNPs and Kao materials, the oxidation peak current increased 3-fold compared to the SPCE, and the peak shape enhanced. Therefore, the Kao–GNPs/SPCE sensor was used for the electroanalytical determination of PROP.

3.2 Optimization of the sensor

$HAuCl_4$ concentration, number of cycles, and amount of Kao were optimized by CV to the highest oxidation peak currents and peak shape of PROP. $HAuCl_4$ concentration was changed in the concentration range of 0.01–0.3 mM (Fig. S2a). The peak current intensities obtained with different concentrations were compared to selected 0.1 mM $HAuCl_4$ as the optimum concentration. The number of cycles was changed from 5 to 20 (Fig. S2b). The optimum number of cycles was selected as 15 cycles. The amount of Kao mineral clay was optimized (Fig. S2c) in the range between 0.5% and 2.0%. The amount of optimum was selected as 1.0%.

Electrochemical behavior of PROP on Kao – GNPs/SPCE

The electrochemical behavior of PROP was investigated by the CV method 1.0 M acetate buffer pH 4.5. Figure 4 represents the CVs of 100.0 µM PROP at the scan rates between 25 and 400 mV/s. As shown in Fig. 4, there is an oxidation peak at about 0.78 V; in the reverse scan, there is no corresponding reduction peak. This situation confirms that the electro-oxidation of PROP exhibits irreversible oxidation behavior [25]. The logi_p – log graph was plotted in different scan rates. The slope of the logi_p – log graph is

about 0.77, indicating the dominant adsorption-controlled electrochemical process [26, 27]. The electro-oxidation of PROP is likely to occur with the loss of one electron, which means the oxidation of tertiary nitrogen in the aromatic ring to a radical cation [25].

3.3 Electrochemical method development and validation

The DPV voltammograms were recorded in the range between 0.01 and 500 μM under the optimum conditions (Fig. 5). As seen from the calibration curves, two different linear working ranges for PROP were observed (0.012–1.0; 1.0–500.0 μM).

The limit of detection (LOD), the limit of quantification (LOQ), and linear working ranges were calculated using a calibration curve [28]. The detection limit was 0.0036 μM, and the LOQ value was 0.012 μM. All validation and regression parameters are represented in Table 1. There is no data relating to individual quantification of PROP in the literature. These results demonstrated that the sensor exhibited good repeatability and reproducibility values.

The obtained LOD and LOQ values offer better detection limits than the literature data [25].

The proposed sensor's repeatability, reproducibility, and stability were also investigated based on the DPV signal of the 30.0 μM PROP. The intra-day peak potential and current repeatability of the sensor were examined with five different measurements, and the related RSD% values indicating the perfect repeatability were obtained 1.09 and 2.28, respectively.

The reproducibility of the Kao–GNPs/SPCE was carried out using five different sensors that were prepared similarly. The DPV current responses were recorded to calculate the RSD% values based on the peak potential and current of PROP. The corresponding RSD% values are given in Table 1, demonstrating the excellent reproducibility of the sensor.

Table 1
Regression data of the calibration lines of PROP on Kao–GNPs/SPCE sensor

Regression parameters	PROP
Linear working range, μM	0.012–1.0; 1.0–500.0
Limit of detection (LOD), μM	0.0036
Limit of quantification (LOQ), μM	0.012
Regression coefficient (R^2)	0.99; 0.99
Reproducibility of peak potential, RSD%[a]	1.37
Reproducibility of peak current, RSD%[a]	1.62
Repeatability of peak potential, RSD%[a] (intra-day)	1.09
Repeatability of peak current, RSD%[a] (intra-day)	2.28

[a]RSD is the relative standard deviation of 5 replications.

The stability of the Kao–GNPs/SPCE sensor was examined using the redox probe $Fe(CN)_6^{3-/4-}$ by recording ten successive CV cycles (Fig. S3). The RSD% values obtained are given in Table S1, confirming the respectable stability of the Kao–GNPs/SPCE sensor.

3.4 Interference study

The probable interference effect of different interfering compounds, namely, Dopamine, Uric acid, L-glycine, Ascorbic acid, Glucose, Na_3PO_4, KCl, Mg (II), and Ca (II) was studied by DPV measurements. The concentration of interfering species with respect to PROP was 1:1. The interferences induced by each species were below 3.1% (Fig. S4).

3.5 Real sample analysis

The commercial human serum sample was used to test the applicability of the proposed sensor in biological samples for PROP analysis. As the sampling procedure is given in Section 2.4, the serum sample was spiked into the solution containing 30.0 μM PROP in acetate buffer, pH 4.5. Then the DPV responses were recorded and evaluated with the linear regression equation of the calibration graph to calculate the recovery results. Table 2 represents the recovery results of three repetitive experiments of 30.0 μM PROP. According to Table 2, the average recovery value was found as 99.43% with a very low RSD% indicating the perfect applicability of the proposed Kao–GNPs/SPCE sensor for PROP analysis in the biological medium.

Table 2
Recovery results in the human serum sample

Real Sample	Method	Sample	Added amount, µM	Found amount, µM	Average recovery, %	RSD[a], %
Human serum sample	DPV	PROP	30.0	29.83 ± 0.437	99.43 ± 1.457	1.465

[a]Each value is the mean of three experiments (95% Confidence Level).

3.6 (dsDNA)-PROP interaction studies

The ds-DNA interaction of PROP with calf thymus ds-DNA in acetate buffer pH 4.5 was investigated by the DPV method on Kao–GNPs/SPCE sensor surface. The increasing concentration of ds-DNA (1.0 to 10.0 ppm) was added to the solution containing 200.0 µM PROP. The peak current and potential changes of PROP were evaluated (Fig. 6). With increasing concentration of ds-DNA, the peak current of PROP decreased. This situation confirms the ds-DNA-PROP interaction [29, 30]. This interaction in solution may occur as a complex formation reaction given below:

mPROP + DNA $\leftrightarrow$ PROP-DNA

The binding constant of this equilibrium can be calculated using voltammetric data based on the literature equations given:

$$log\frac{1}{[DNA]} = logK + mlog\frac{i_{PROP-DNA}}{i_{PROP} - i_{PROP-DNA}}$$

1

In Eq. (1), K symbolizes the PROP-DNA binding constant,i_{PROP} and $i_{\text{PROP–DNA}}$ denotes the current values of free PROP and the PROP-(ds-DNA) complex, respectively. [DNA] means ds-DNA concentration, and m indicates the binding ratio [31–33]. Because Eq. (1) shows a linear regression between $log\frac{1}{[DNA]}$ and $log\frac{i_{PROP-DNA}}{i_{PROP}-i_{PROP-DNA}}$ (given in the inset of Fig. 6), the antilogarithm of the intercept displays the PROP-DNA binding constant (K), and the slope represents the binding ratio. Eq. (1) shows that the intercept and slope were found as 4.33 and 0.98 (inset of Fig. 6). The binding constant of the PROP-(ds-DNA) complex was calculated as 2.14 (± 0.42) × 10^4 M^{-1}. The binding ratio was approximately 1.0, indicating the 1:1 complex formation of PROP and ds-DNA [31, 32]. The K value is comparable with the literature data for some similar ds-DNA-drug complexes (between 10^4 and 10^6 M^{-1}) [34, 35]. The relative order of the K value indicates that the PROP-(ds-DNA) complex formation may be intercalative [36, 37].

For calculating the Gibbs free energy (ΔGº) of PROP-(ds-DNA) complex formation, Eq. (2) is used:

ΔGº = −RTlnK (2)

R, T, and K are used in their usual denotations here.

We found ΔG° = − 24.70 kJ/mol by substituting K for the experimental value given above and taking T as 298 K. As a result, the complex-formation reaction occurs spontaneously [30, 34].

4 Conclusion

Natural kaolinite mineral–gold nanoparticles/screen printed carbon electrode were prepared with a simple, cost-effective surface modification by two steps for the electrochemical analysis of PROP. The real sample application of the sensor was performed successfully in a commercial human serum sample without any interference effect of Ca (II), Mg (II), Dopamine, Uric acid, Na_3PO_4, KCl, L-Glycine, Ascorbic acid, and Glucose. The interactions between PROP and ds-DNA were studied using the voltammetric signal of PROP for the first time. A 1:1 complex of intercalative nature was formed between ds-DNA and PROP. The thermodynamic parameters Gibbs free energy (G) and binding constant (K) of the interaction were also calculated as − 24.70 kJ/mol, 2.14 (± 0.42) × 10^4 M^{-1}, respectively.

Declarations

CRediT authorship contribution statement

Ceren Yıldız: Methodology, Software, Drafting the article**, Dilek Eskiköy Bayraktepe:** Methodology, Software, Investigation, Data collection, writing - review & editing. **Zehra Yazan:** Supervision, Design of the work, Writing - review & editing.

Declaration of Competing Interest

The authors declare that they have no known competing financial
interests or personal relationships.

Data availability

Data will be available on request

Acknowledgments

The authors thank the Ankara University Research Fund with project number 20L0430001 for the financial support.

References

1. Gergov G, Alin A, Katsarov P, Simeonov V, Yankov D, Al-Degs Y (2018) Net analyte signal-based methods for the simultaneous determination of paracetamol, propyphenazone and caffeine by UV spectrophotometry. Bulg Chem Commun 50(2):265–273

2. Burdan F (2004) Developmental effects of propyphenazone in analgesic and antipyretic combination with caffeine or paracetamol. Hum Exp Toxicol 23(5):235–244. https://doi.org/10.1191/0960327104ht439oa
3. Boerlin V, Maeglin B, Hägler W, Kuhn M, Nüesch E (1986) Analgesic activity of propyphenazone in patients with pain following oral surgery. Eur J Clin Pharmacol 31:127–131. https://doi.org/10.1007/BF00606648
4. Santoni G, Fabbri L, Gratteri P, Renzi G, Pinzauti S (1992) Simultaneous determination of aspirin, codeine phosphate and propyphenazone in tablets by reversed-phase high-performance liquid chromatography. Int J Pharm 80(1–3):263–266. https://doi.org/10.1016/0378-5173(92)90284-9
5. Rouan M, Campestrini J, Lecaillon J, Godbillon J (1992) Rapid determination of propyphenazone in plasma by high-performance liquid chromatography. J Chromatogr B Biomed Sci Appl 577(2):387–390. https://doi.org/10.1016/0378-4347(92)80265-R
6. Rohman A, Dzulfianto A, Riswanto FDO (2017) The employment of UV-spectroscopy combined with multivariate calibration for analysis of paracetamol, Propyphenazone and caffeine. Indones J Pharm 28(4):191. http://dx.doi.org/10.14499/indonesianjpharm28iss4pp191
7. Scholz F (2015) Voltammetric techniques of analysis: the essentials. ChemTexts 1(4):17. https://doi.org/10.1007/s40828-015-0016-y
8. Porada R, Jedlińska K, Lipińska J, Baś B (2020) Voltammetric sensors with laterally placed working electrodes: A review. J Electrochem Soc 167(3):037536. https://doi.org/10.1149/1945-7111/ab64d6
9. David IG, Buleandra M, Popa DE, Cheregi MC, David V, Iorgulescu EE, Tartareanu GO (2022) Recent developments in voltammetric analysis of pharmaceuticals using disposable pencil graphite electrodes. Processes 10(3):472. https://doi.org/10.3390/pr10030472
10. Couto R, Lima J, Quinaz M (2016) Recent developments, characteristics and potential applications of screen-printed electrodes in pharmaceutical and biological analysis. Talanta 146:801–814. https://doi.org/10.1016/j.talanta.2015.06.011
11. Trojanowicz M, Mulchandani A, Mascini M (2004) Carbon nanotubes-modified screen-printed electrodes for chemical sensors and biosensors. Anal Lett 37(15):3185–3204. https://doi.org/10.1081/AL-200040320
12. Buffon E, Stradiotto NR (2021) A molecularly imprinted polymer on reduced graphene oxide-gold nanoparticles modified screen-printed electrode for selective determination of ferulic acid in orange peels. Microchem J 167:106339. https://doi.org/10.1016/j.microc.2021.106339
13. Gupta A, Sharma AL, Deep A (2021) Sensitive impedimetric detection of E. coli with metal-organic framework (MIL-53)/polymer (PEDOT) composite modified screen-printed electrodes. J Environ Chem Eng 9(1):104925. https://doi.org/10.1016/j.jece.2020.104925
14. Shih Y, Zen J-M, Yang H-H (2002) Determination of codeine in urine and drug formulations using a clay-modified screen-printed carbon electrode. J Pharm Biomed Anal 29(5):827–833. https://doi.org/10.1016/S0731-7085(02)00179-6

15. Murray HH (2006) Structure and composition of the clay minerals and their physical and chemical properties. Dev Clay Sci 2:7–31. https://doi.org/10.1016/S1572-4352(06)02002-2
16. Brown G (1984) Crystal structures of clay minerals and related phyllosilicates. Philos Trans Royal Soc A 311(1517):221–240. https://doi.org/10.1098/rsta.1984.0025
17. Akanji SP, Arotiba OA, Nkosi D (2019) Voltammetric determination of Pb (II) ions at a modified kaolinite-carbon paste Electrode. Electrocatalysis 10:643–652. https://doi.org/10.1007/s12678-019-00552-3
18. Phongphut A, Chayasombat B, Cass AE, Sirisuk A, Phisalaphong M, Prichanont S, Thanachayanont C (2020) Clay/au nanoparticle composites as acetylcholinesterase carriers and modified-electrode materials: A comparative study. Appl Clay Sci 194:105704. https://doi.org/10.1016/j.clay.2020.105704
19. Williams AK, Dasilva SC, Bhatta A, Rawal B, Liu M, Korobkova EA (2012) Determination of the drug–DNA binding modes using fluorescence-based assays. Anal Biochem 422(2):66–73. https://doi.org/10.1016/j.ab.2011.12.041
20. Sirajuddin M, Ali S, Badshah A (2013) Drug–DNA interactions and their study by UV–Visible, fluorescence spectroscopies and cyclic voltametry. J Photochem Photobiol B Biol 124:1–19. https://doi.org/10.1016/j.jphotobiol.2013.03.013
21. Urçuk A, Bayraktepe DE, Yıldız C, Yazan Z (2022) Kinetic and thermodynamic studies on the interaction between calf thymus DNA and food additive vanillin-electrochemical methods. J Mol Liq 360:119434. https://doi.org/10.1016/j.molliq.2022.119434
22. Hezard T, Fajerwerg K, Evrard D, Collière V, Behra P, Gros P (2012) Gold nanoparticles electrodeposited on glassy carbon using cyclic voltammetry: Application to Hg (II) trace analysis. J Electroanal Chem 664:46–52. https://doi.org/10.1016/j.jelechem.2011.10.014
23. Bayraktepe DE, Yıldız C, Yazan Z (2023) The development of electrochemical DNA biosensor based on poly-l-methionine and bimetallic AuPt nanoparticles coating: Picomolar detection of Imatinib and Erlotinib. Talanta 257:124361. https://doi.org/10.1016/j.talanta.2023.124361
24. Erden S, Yazan Z (2018) A New Sepiolite Clay/TiO_2/multiwall carbon nanotube modified carbon paste sensor for the adsorptive stripping square wave voltammetric analysis of vanillin in local food samples. Rev Roum Chim 63:977–986
25. Silva WP, Silva LA, França CH, Sousa RM, Muñoz RA, Richter EM (2017) Square-wave Voltammetric Determination of Propyphenazone, Paracetamol, and Caffeine: Comparative Study between Batch Injection Analysis and Conventional Electrochemical Systems. Electroanalysis 29(8):1860–1866. https://doi.org/10.1002/elan.201700160
26. Borowiec J, Wei L, Zhu L, Zhang J (2012) Multi-walled carbon nanotubes modified glassy carbon electrode for sensitive determination of ketoconazole. Analy Methods 4(2):444–448. https://doi.org/448
27. Aydar S, Bayraktepe D, Filik H, Yazan Z (2020) Low-level electrochemical analysis of ketoconazole by sepiolite nanoparticles modified sensor in shampoo sample. Acta Chim Slov 67(3).

https://doi.org/10.17344/acsi.2019.5398
28. Tüzün ÜN, Yıldız C, Eskikoey Bayraktepe D, Polat K, Yazan Z (2023) Electrochemical fabrication of poly (L-alanine)-gold nanoparticle nanocomposite-modified electrode: application for determination and mechanism of antipsychotic drug olanzapine. Monatsh Chem 154(1):95–104. https://doi.org/10.1007/s00706-022-03012-9
29. Shahabadi N, Moghadam NH (2012) Determining the mode of interaction of calf thymus DNA with the drug sumatriptan using voltammetric and spectroscopic techniques. Spectrochim Acta A Mol Biomol Spectrosc 99:18–22. https://doi.org/10.1016/j.saa.2012.09.022
30. Bayraktepe DE (2020) A voltammetric study on drug-DNA interactions: Kinetic and thermodynamic aspects of the relations between the anticancer agent dasatinib and ds-DNA using a pencil lead graphite electrode. Microchem J 157:104946. https://doi.org/10.1016/j.microc.2020.104946
31. Ni Y, Wang Y, Kokot S (2010) Voltammetric, UV–vis spectrometric and fluorescence study of the interaction of ractopamine and DNA with the aid of multivariate curve resolution-alternating least squares. Electroanalysis 22(19):2216–2224. https://doi.org/10.1002/elan.200900596
32. Kalanur SS, Katrahalli U, Seetharamappa J (2009) Electrochemical studies and spectroscopic investigations on the interaction of an anticancer drug with DNA and their analytical applications. J Electroanal Chem 636(1–2):93–100. https://doi.org/10.1016/j.jelechem.2009.09.018
33. Morawska K, Popławski T, Ciesielski W, Smarzewska S (2020) Interactions of lamotrigine with single- and double-stranded DNA under physiological conditions. Bioelectrochemistry 136:107630. https://doi.org/10.1016/j.bioelechem.2020.107630
34. Temerk Y, Ibrahim M, Ibrahim H, Kotb M (2016) Interactions of an anticancer drug lomustine with single and double stranded DNA at physiological conditions analyzed by electrochemical and spectroscopic methods. J Electroanal Chem 769:62–71. https://doi.org/10.1016/j.jelechem.2016.03.020
35. Bi S, Zhang H, Qiao C, Sun Y, Liu C (2008) Studies of interaction of emodin and DNA in the presence of ethidium bromide by spectroscopic method. Spectrochim Acta A Mol Biomol Spectrosc 69(1):123–129. https://doi.org/10.1016/j.saa.2007.03.017
36. Nawaz H, Rauf S, Akhtar K, Khalid AM (2006) Electrochemical DNA biosensor for the study of ciprofloxacin–DNA interaction. Anal Biochem 354(1):28–34. https://doi.org/10.1016/j.ab.2006.04.004
37. Pandit UJ, Naikoo GA, Khan GA, Wankar S, Khan I KK R and SN L ISSN 0975-413X CODEN (USA): PCHHAX

Figures

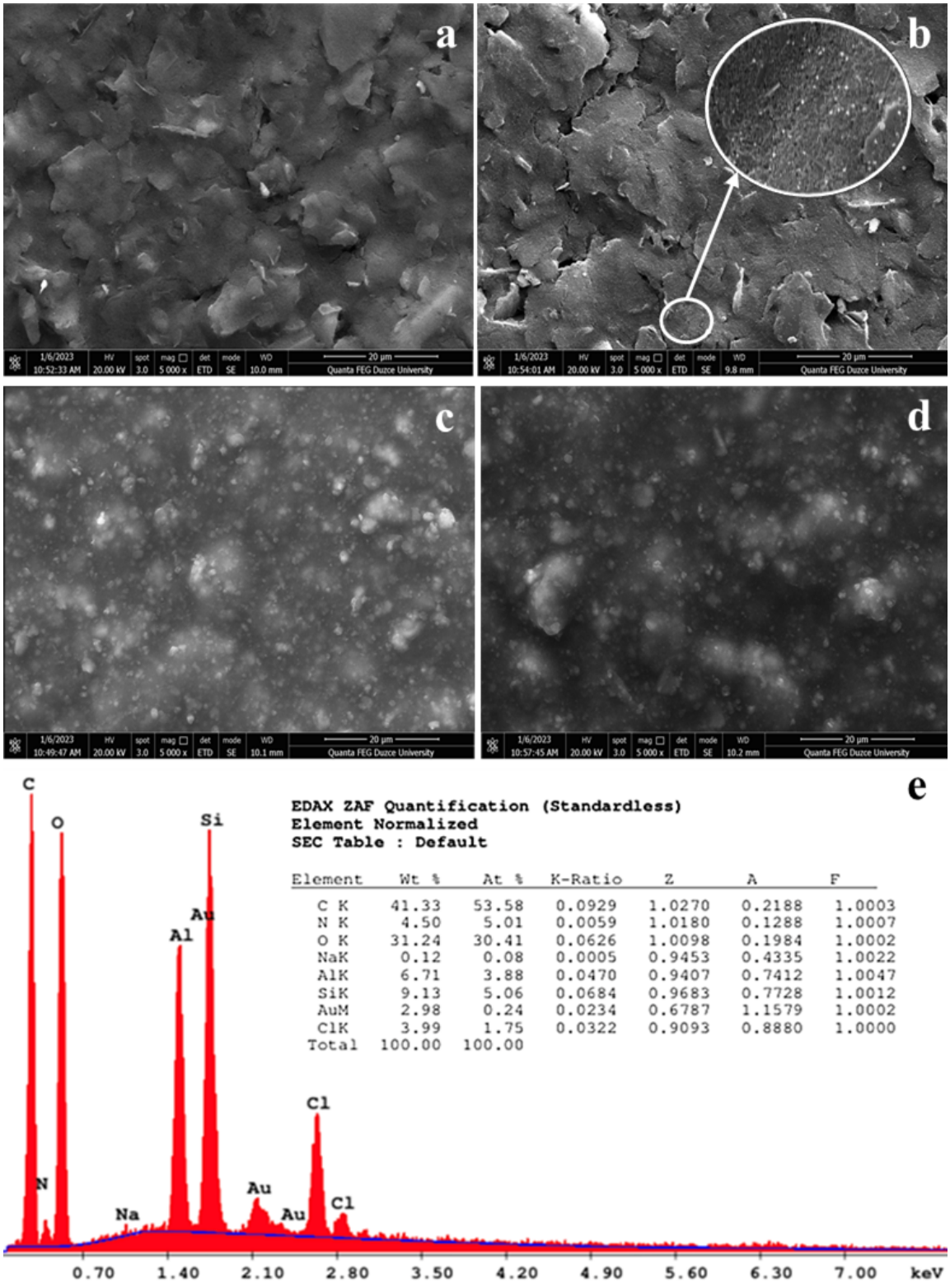

Figure 1

FE-SEM images of (**a**) SPCE, (**b**) GNPs/SPCE, (**c**) Kao/SPCE, (**d**) Kao–GNPs/SPCE, and **e** EDS spectrum of Kao–GNPs/SPCE

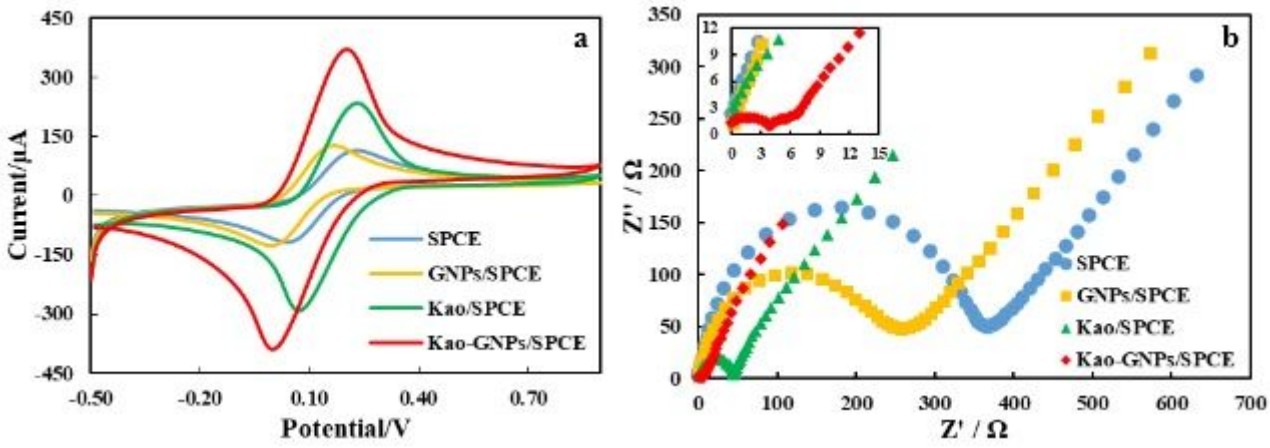

Figure 2

(**a**) Cyclic voltammograms, (**b**) Nyquist diagrams of 5.0 mM of $[Fe(CN)_6]^{3-/4}$ in 0.1 M KCl solution on SPCE, GNPs/SPCE, Kao/PGE, and Kao–GNPs/SPCE at a scan rate of 0.05 Vs^{-1} (R_{ct}: The charge transfer resistance, W: Warburg element, R_s: The cell resistance, C_{dl}: the capacitance of the double layer)

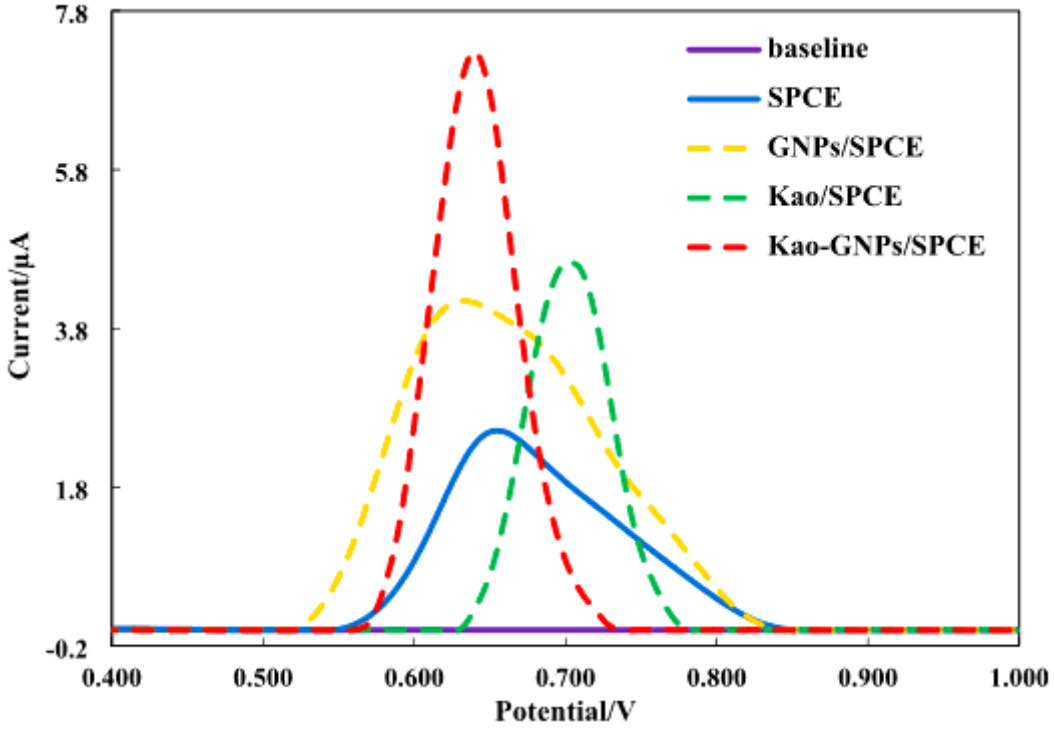

Figure 3

DPV voltammograms of the different modified SPCE sensors for 30.0 μM PROP in pH 4.5 ABS buffer solution

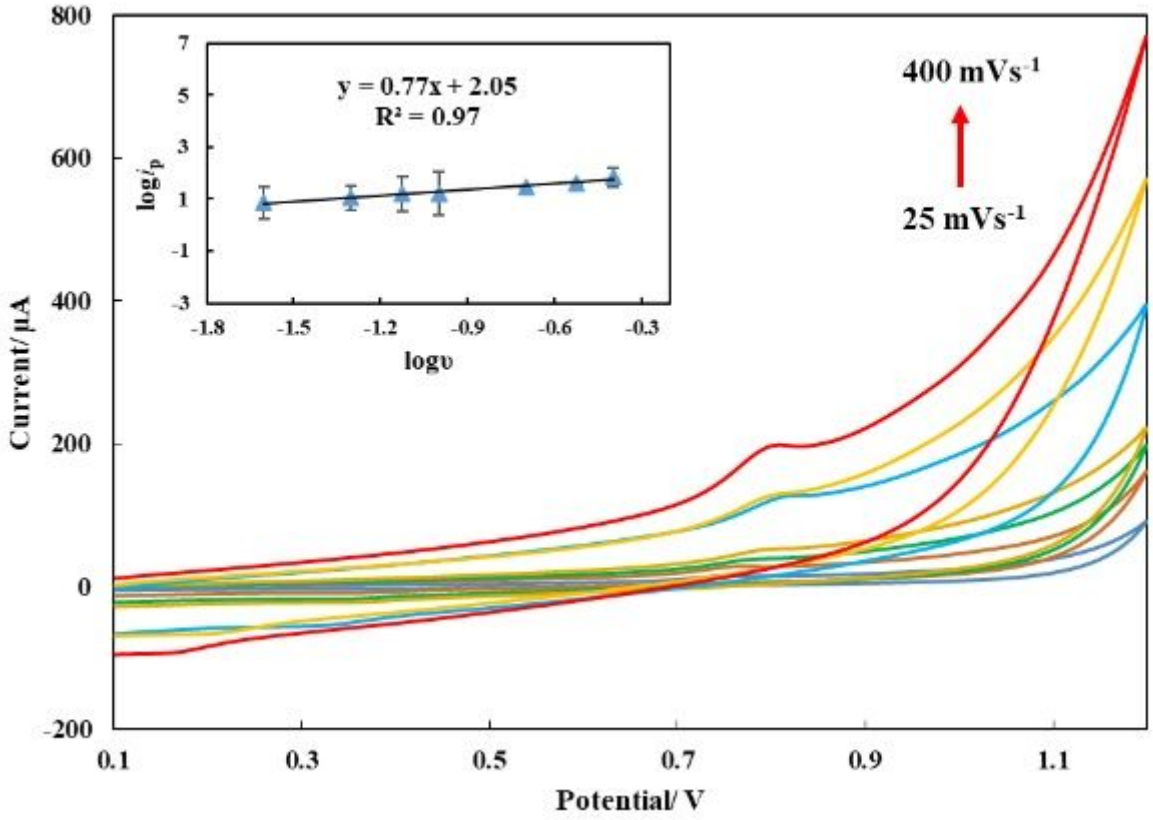

Figure 4

CV voltammograms of 100.0 µM PROP at different scan rates (0.025 – 0.4 Vs^{-1}) in ABS buffer solution, pH 4.5 **Insets:** logi_p – log graphs of PROP

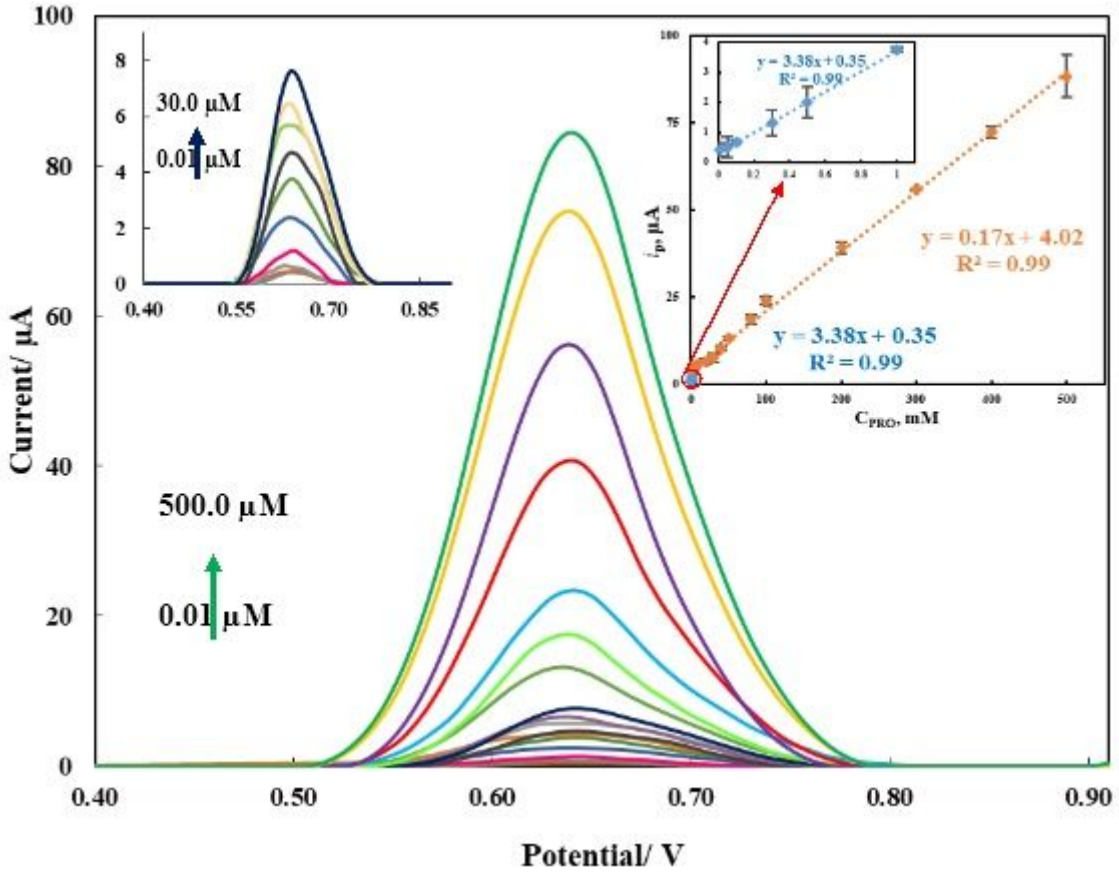

Figure 5

DPVs of PROP determination using Kao–GNPs/SPCE sensor in pH 4.5 ABS buffer solution **Insets:** Plots of peak current vs. concentrations of PROP

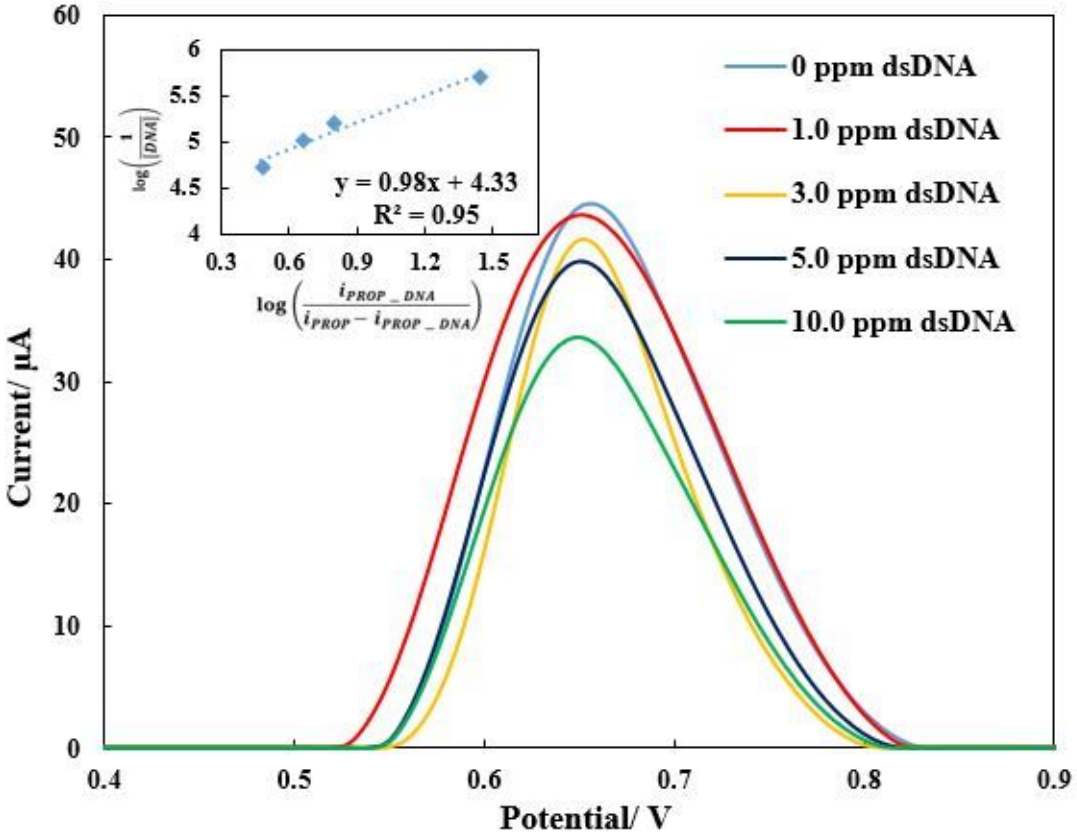

DPV voltammograms of 200.0 µM PROP with increasing concentration of ds-DNA in acetate buffer solution pH 4.5 **Insets:** $\log\left(\frac{i_{PROP-DNA}}{i_{PROP}-i_{PROP-DNA}}\right)$ – $\log\left(\frac{1}{[DNA]}\right)$ graphs

Figure 6

See image above for figure legend

Supplementary Files

This is a list of supplementary files associated with this preprint. Click to download.

- SupplementaryFile.docx